Mean wind and its reversal in thermal convection

K. R. Sreenivasan*
Mason Laboratory, Yale University, New Haven, Connecticut 06520-8286

A. Bershadskii
ICAR, P. O. Box 31155, Jerusalem 91000, Israel
and Yale University, New Haven, Connecticut 06520-8286

J. J. Niemela
Cryogenic Helium Turbulence Laboratory, Department of Physics, University of Oregon, Eugene, Oregon 97403
(Received 20 December 2001; published 8 May 2002)

Properties of the mean wind in thermal convection, especially the abrupt reversal of its direction at high Rayleigh numbers, are studied. Measurements made in a closed cylindrical container of aspect ratio 1 are analyzed, and both the long-term and short-term behaviors of the direction reversals are discussed. A first look at the data suggests a Brownian-type process in action, but a closer look suggests the existence of hierarchical features with time scales extending roughly over a decade and a half. A physical model consistent with experimental observations is presented, and the origin of the cutoff scales is discussed. It appears that the generation of the wind as well as the reversal of its direction can be understood in terms of the imbalance between buoyancy effects and friction.

DOI: 10.1103/PhysRevE.65.056306 PACS number(s): 47.27.Jv, 47.27.Nz, 47.27.Te

I. INTRODUCTION

A. General

Consider a closed cylindrical container whose aspect ratio (the ratio of the diameter to its height) is of order unity. The bottom wall is heated uniformly and the top wall similarly cooled, and a steady temperature difference Δ is maintained between them. The sidewall is nominally nonconducting. The fluid inside the container undergoes thermal convection if the Rayleigh number exceeds a critical value. The Rayleigh number, defined as $\mathrm{Ra}=\alpha_p \Delta g H^3/\nu\kappa$, is a nondimensional measure of the temperature difference Δ. Here, α_p is the isobaric thermal expansion coefficient, ν the kinematic viscosity, and κ the thermal diffusivity of the fluid; g is the acceleration due to gravity and H is the vertical distance between top and bottom walls of the container. The Rayleigh numbers considered in this paper lie between about 10^8 and 10^{13}. Convection is turbulent at these Rayleigh numbers, and approaches a fully developed state toward the upper end of the range.

Experiments show that superimposed on the background turbulence is a large-scale recirculating motion, often called the mean wind, whose scale is of the order of the container itself [1–8]. (It is possible that the large-scale circulation observed in Ref. [1] for large aspect ratios is different from the mean wind for aspect ratios of the order unity, as observed in Refs. [2–8].) The mean wind seems to persist at least for several decades of the Rayleigh number and for a variety of Prandtl numbers ($\mathrm{Pr}=\nu/\kappa$). Tentative explanations of the origin of the mean wind as well as its occasional and sudden reversals have been mentioned informally (e.g., Ref. [9]), but serious efforts have not yet been made. Our goal is to make a reasonable beginning. Since similar reversals occur in other contexts such as the magnetic polarity of the earth (e.g., Ref. [10]) and the wind direction in the earth's atmosphere (e.g., Ref. [11]), the problem is of some broad interest.

B. Evidence for the mean wind

The evidence for the wind comes from a variety of sources. First, at Rayleigh numbers of the order 10^9, visualization of water flows (e.g., Refs. [6,12]) directly confirms its existence. Second, at similar Rayleigh numbers, measurement of the fluid velocity along a diameter of the container, made using laser Doppler velocimetry, is consistent with the existence of a mean wind whose center resides at the midpoint on the axis of the container (Refs. [6,12]). At these Rayleigh numbers, however, one may wonder legitimately if the convection is fully turbulent (at least because the boundary layers are essentially laminarlike). For water and other fluids whose Prandtl number is of order unity, it takes Rayleigh numbers of the order of 10^{12} for the boundary layers to become fully turbulent as well [13], and thus for the flow as a whole to be regarded as developed turbulence.

There is evidence that the mean wind exists even when convection is fully turbulent, but this evidence is somewhat indirect. It comes from the simultaneous measurement of temperature from two neighboring probes with known separation distance, situated such that a presumed mean wind would pass one probe a short time after it has passed the other. By making short-time correlation measurements between temperature signals from the two probes for various time delays, and by identifying the time delay that yields the largest correlation, one infers a velocity for the mean wind (e.g., Refs. [3,8]); instead of making correlation measure-

*Present address: Institute for Physical Science and Technology, University of Maryland, College Park, MD 20742.

ments, one can obtain equivalent data through short-term spectra (e.g., Ref. [14]). In either case, the inference is that the mean wind exists. To the first order, this inferred velocity scales in the same way as that directly measured at lower Rayleigh numbers (see, e.g., [15]), so it is conceivable that the wind velocity that one observes directly at lower Rayleigh numbers persists also to higher Rayleigh numbers of the order of 10^{13}. What happens at even higher Rayleigh numbers is unclear because the short-term correlation method of measurement becomes operationally unreliable; whether a more suitable method of measurement would be better able to discern the mean wind, or the mean wind breaks up and becomes substantially weaker, is at present unclear.

Before proceeding further, it is useful to present a few facts about the wind. The first obvious fact is that the observed wind has a different symmetry from what might be expected naively from the circular cross section of the container. The geometry of the container might suggest a torus with a single overturning motion, but it is known from large aspect ratio circular containers that this is not the preferred mode. Indeed, there, as here, the realized motion apparently consists of straight roll-like structures. In a circularly symmetric configuration a single such roll could be expected to exhibit azimuthal drift (or ''jitter''), and a certain amount of wandering is indeed observed in experiments. However, a fixed orientation is maintained by and large—and it is presumably determined by a variety of small variables in a given apparatus, as well as initial conditions of start-up; perhaps a benign condition such as a welding seam might be an adequate anchor. These aspects are not fully understood at present. In some cases a slight tilt has been applied to the apparatus to firmly fix the orientation of the wind (e.g., Refs. [12,16]). An experimenter measuring with a few probes has no means of knowing *a priori* the orientation of the mean wind with respect to the probes, and so different measurements at the same Rayleigh number could be expected to obtain somewhat different numbers for the magnitude of the mean wind. These differences depend on the angle θ between the probe and the axis of the mean wind (presumably varying as $\cos\theta$); as long as θ is not too large, the variations are not expected to be orders of magnitude in extent.

C. The reversal of the wind direction

The aspect that concerns us here most is that the mean wind undergoes an occasional and relatively sudden reversal of its direction. The source for this inference is Fig. 1, where the mean wind is plotted as a function of time for the Rayleigh number of 1.5×10^{11}. It should be immediately noted that an equally valid interpretation of Fig. 1 is that the mean wind abruptly rotates by 180° azimuthally; the effect on the fixed probe is the same as if the wind reversed its direction. The azimuthal rotation may appear to be more appealing from symmetry considerations, but since most of the action in thermal turbulence is in the direction of gravity, and large thermal perturbations are the norm in the turbulent state, the reversal of direction may appear to be the more natural occurrence. For simplicity, we shall refer to the observed phenomenon as the reversal of direction without being specific until Sec. IV. It is clear from Fig. 1 that the wind reverses direction with no particular regularity; it is abrupt on the scale of a characteristic turnover time.

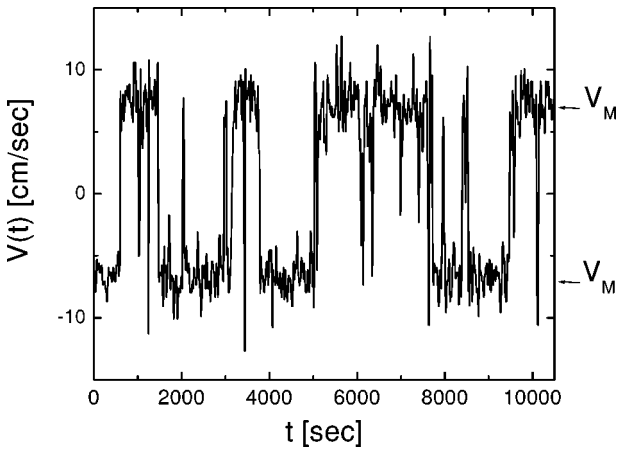

FIG. 1. The wind velocity as a function of time, obtained by correlating two neighboring temperature probes on the center plane of the convection cell, about 4.4 cm away from the wall, outside the sidewall boundary layers. $\mathrm{Ra}=1.5\times10^{11}$. The wind switches direction abruptly with no apparent order. The arrows on the right indicate the magnitude of the wind during its persistence in one direction.

The duration of the record in Fig. 1 is about 3 h. In order to obtain reliable statistics, we have obtained a contiguous record lasting 5.5 days. These measurements were begun after the apparatus had been kept at constant experimental conditions for nearly a month, resulting in a very stable initial state. The arrows to the right of Fig. 1 give reasonably unambiguous estimates of the mean wind speed V_M, which is the same to a good approximation for its two orientations.

Perhaps a somewhat different interpretation of the mean wind may be mentioned, though we shall not consider this further. Qiu and Tong [12] imagine that there is no continuous mean wind but only up and down fluid motions coordinated along the wall, with the mass balance presumably satisfied by an uncoordinated down and up motion toward the middle of the container. Under this scenario, the information along the top and bottom walls is communicated instantly by means of pressure pulses, so in this sense too there is a correlated activity along the entire perimeter. This kind of motion was earlier considered theoretically by Villermaux [17].

D. The plan of the paper

In Sec. II, we shall describe some details of the experimental apparatus and the flow, and note a few basic properties of the wind. Section III shows that the wind reversal appears to be a Brownian process to first order, but that a closer scrutiny reveals a long-term dependence with a hierarchy of self-similar scales in a certain range, and a rough correspondence to self-organized criticality. In Sec. IV, the results are interpreted in a broad framework as well as in physical terms. The paper concludes with summary remarks in Sec. V.

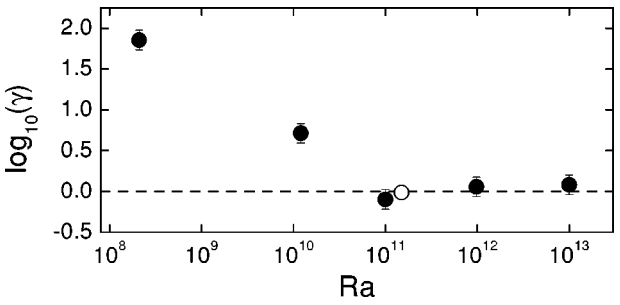

FIG. 2. The magnitude of the logarithm of the reversal factor γ as a function of Ra. For $\mathrm{Ra}>10^{11}$, the wind seems to have no preference for one direction over the other, except that the frequency with which it switches direction increases (see Ref. [8]). The closed symbols are from 3 h of data, the open symbol from 131 h.

II. PRELIMINARY DETAILS

A. The apparatus and some experimental conditions

The apparatus was the same as that used previously by Niemela *et al.* [8], itself a modification of the apparatus used in Ref. [18]. A few salient features are noted here. The working fluid was cryogenic helium gas. The apparatus was a circular cylinder of 50 cm diameter and 50 cm height; the aspect ratio Γ, defined as D/H, was thus unity. The top and bottom plates of the apparatus were made of copper annealed under oxygen-free conditions; the thermal conductivity of this copper was large and of the order of 2 $\mathrm{kW\,m^{-1}\,K^{-1}}$ at a temperature of 5 K. The thickness of these plates was 3.8 cm, and the surface finish was better than 10 μm. Specially designed thin metal film heaters were attached to the back of each copper plate by dilute varnish, and sandwiched by an additional copper plate of 0.16 cm thickness. A constant heat flux occurred at the bottom plate whenever experimental conditions were altered, but measurements were begun in the steady state only after a constant temperature was reached. The top wall was connected to a helium reservoir through a distributed and adjustable thermal link, and its temperature was maintained constant by means of a resistance bridge and servo.

The lateral confinement of the fluid was achieved with type 304 stainless steel of thickness 0.267 cm. The convection cell was insulated by three thermal shields at various graded temperatures, residing in a common vacuum space. The conductivity of stainless steel at the operating temperature (see Ref. [19]) is approximately 0.25 W/m K.

B. The Rayleigh number variation of the wind

At $\mathrm{Ra}=1.5\times10^{11}$, to which Fig. 1 refers, the wind is as often in one direction as in the other (to within about 1.4% over the duration of the experiment). At lower Ra, however, the wind favors one direction over the other. Figure 2 shows the tendency of the wind to reverse its direction: the "reversal factor" γ is the ratio of time that the wind is in one direction compared to that in the opposite direction. This factor is unity when there is no average preference for one direction over the other. The onset of reversals occurs at Ra somewhere below about 10^8, but this onset value depends on various experimental conditions (see Sec. IV C). For $\mathrm{Ra}>10^{11}$, the wind prefers no particular direction; however, as shown in Ref. [8], it switches directions increasingly more often until, toward a Ra of 10^{13}, it becomes difficult to distinguish it from background fluctuations. This, as already mentioned, may be a limitation of the method of measurement.

Niemela *et al.* [13] have examined in some detail the variation of the Reynolds number $\mathrm{Re}=V_M H/\nu$ with respect to the Rayleigh number. The summary (see also Ref. [15]) is that

$$\mathrm{Re}=f(\Gamma)\mathrm{Pr}^{-0.7}\,\mathrm{Ra}^{0.49}, \tag{1}$$

where $f(\Gamma)$ is a function of the aspect ratio Γ of the apparatus. For the present experiments with $\Gamma=1$, we find $f(\Gamma)\approx0.2$.

While the measurements spanned a Rayleigh number between 10^8 and 10^{13}, they were most detailed at $\mathrm{Ra}=1.5\times10^{11}$, at which γ was unity. This "transition" Rayleigh number will be the focus of our attention here, although we have examined data at other Rayleigh numbers and make a few brief remarks about them as appropriate. A few operating conditions corresponding to the transition Rayleigh number are now listed. The temperature at the middle of the experimental chamber was 4.65 K, and the pressure 0.28 bar. The temperature difference Δ was fixed to be 0.11 K. The properties of helium corresponding to the center plane conditions of the container were $\alpha=0.25$ $\mathrm{K^{-1}}$, $\nu=4.0\times10^{-3}$ $\mathrm{cm^2/s}$, and $\kappa=5.3\times10^{-3}$ $\mathrm{cm^2/s}$. The thermal conductivity of the fluid was $k_f=9.1\times10^{-3}$ W/m K, but it is effectively enhanced by the factor of the Nusselt number Nu. The measured value of Nu was 320, and the Reynolds number obtained from Eq. (1) was about 10^5.

III. PROPERTIES OF THE WIND AT THE TRANSITION RAYLEIGH NUMBER

A. The Brownian approximation

The first aspect that needs to be understood is a likely correlation between two successive wind direction reversals. One can see from Fig. 1 that the reversal is relatively fast so that, to a first approximation, it can be regarded as an instantaneous process characterized by only one parameter: the moment at which the reversal occurs. Define T_n as the time between an arbitrarily defined origin in time ("zero") and the nth crossing in the wind direction. A plot of T_n versus n is shown in Fig. 3. To a first approximation, for $n>50$ or so, the relationship is linear. This suggests stationarity in T_n; that is, a mean interval between crossings can be defined satisfactorily if one averages over about 50 of them. The deviation from this linear trend is shown in the inset to Fig. 3. This deviation appears stochastic. One can compute the power spectral density of this deviation as well as its probability density function (PDF), both of which are shown in Fig. 4 (the latter as the inset). The spectral roll-off rate is about -1.94, and the PDF is roughly normal.

Normality of the PDF and a -2 roll-off are characteristic of a Brownian process. The deviation of the present spectral

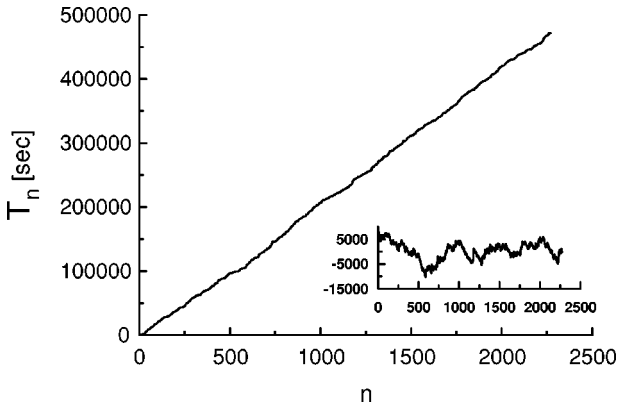

FIG. 3. The dependence of T_n on n observed for Ra$=1.5\times10^{11}$. The linear trend indicates stationarity. Inset shows the same data after removing the linear trend.

shape from the theoretical value of -2 may be understood as a finite-size effect: even though we have acquired data for 5.5 days, the number of crossings is of the order of 2300. Indeed, a Brownian process simulated with this number of points yielded a spectral slope of about -1.92 and a PDF that is very similar to the experimental plot. Thus, it appears reasonable to conclude that the crossing data for the wind direction are approximately Brownian in character.

A tentative conclusion that emerges is that, to a plausible approximation, we have

$$T_n=\langle\tau\rangle n+\delta, \tag{2}$$

where $\langle\tau\rangle$ is the mean interval between two successive crossings and δ, the deviation from the linear trend between T_n and n, is essentially Brownian. This suggests that, at this level of detail, a given reversal of the wind direction does not remember the previous event. The situation is similar to that of the wind-direction changes in the atmosphere analyzed in Ref. [11].

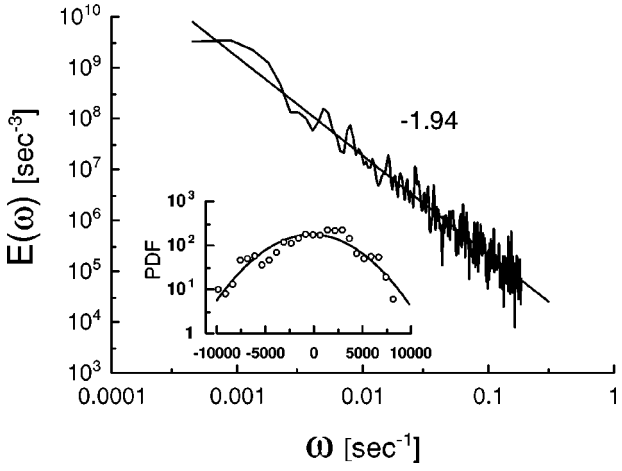

FIG. 4. The spectral density $E(\omega)$ of the random process represented in the inset of Fig. 3. The inset of this figure shows the PDF of this random process; the best parabolic fit shows a normal distribution with the same mean and variance as the data.

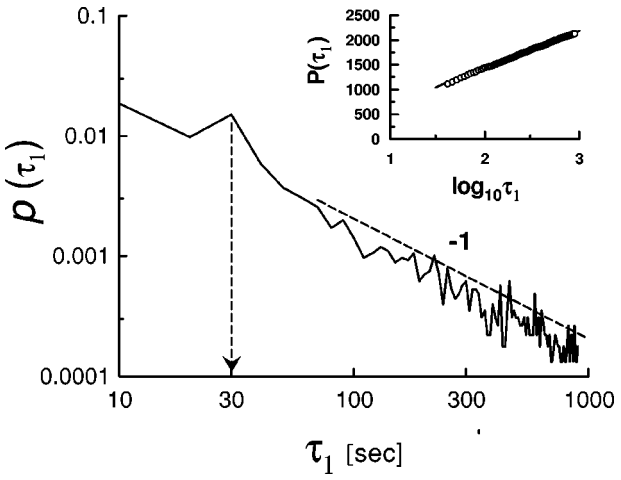

FIG. 5. The PDF $p(\tau_1)$ plotted versus τ_1. The dashed line indicates a power law with a slope of -1. The inset shows the corresponding cumulative distribution; the straight line fit to the data confirms the power-law PDF with the exponent -1.

A more detailed analysis shows that the wind reversals (or ''direction switchings'') possess a more complex structure. Let us define the time interval between the $(n+r)$th and nth reversals as

$$\tau_r\equiv\Delta T_r=T_{n+r}-T_n. \tag{3}$$

For $r=1$ this is simply the gap between adjacent switches, which is the basic interswitch interval. For $r=2$, ΔT_2 is the return time. For arbitrary r, ΔT_r will be called the generalized interswitch interval.

Figure 5 shows the PDF of τ_1 in log-log coordinates. The two important characteristics of the PDF are its peak at $\tau_L=30$ s and the existence of a nearly -1 power law for larger values of τ_1. The peak corresponds to the average time taken for the mean wind (~7 cm/s) to traverse the circumference of the apparatus (~200 cm). The apparent power law is surprising in light of the Brownian behavior discussed earlier for T_n, but its presence over a decade of time scales is unmistakable. To check that the power-law exponent is indeed close to -1, we have calculated the cumulative distribution $P(\tau_1)$,

$$P(\tau_1)=\int_0^{\tau_1}p(\tau')d\tau'. \tag{4}$$

For a PDF with an inverse dependence on τ_1, one has $P(\tau_1)\sim\ln\tau_1$. The inset to Fig. 5 confirms the expected logarithmic behavior of P over the interval of scales for which the PDF shows the -1 slope.

We have evaluated the PDF for return times as well (i.e., for $r=2$) and found a similar -1 power law. For brevity, we will not display the results here.

Obviously, the -1 power law cannot extend to arbitrarily large values of τ_1, and a rapid cutoff can be expected beyond a point where the intervals between switchings become very long. Figure 6 shows that the PDF for large τ_1 is an exponential given by

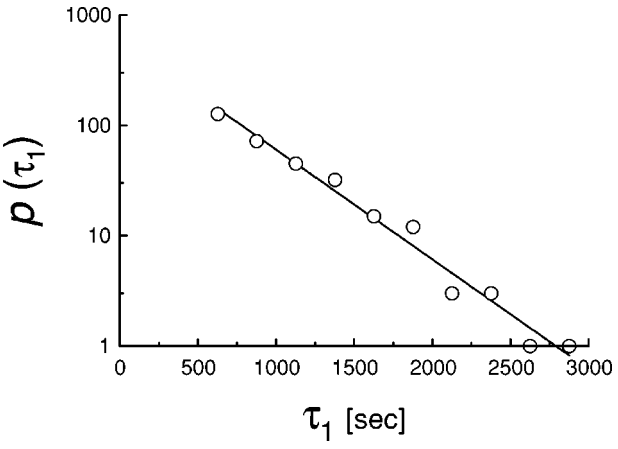

FIG. 6. The PDF of the interswitch intervals ($r=1$) versus τ_1 for large values of τ_1; Ra$=1.5\times10^{11}$. The solid straight line indicates an exponential distribution.

$$p(\tau_1)\sim e^{-\tau_1/\tau_m}. \tag{5}$$

The slope of the straight line gives a new characteristic time scale $\tau_M \simeq 400$ s.

The exponential PDF is typical for Poisson processes. To substantiate this claim, we have also calculated the PDF of the *increments* of the interswitch intervals, $\Delta\tau_1$ (defined as the difference between neighboring values of τ_1); for a true Poisson process, the PDF of the increments is also exponential with the same characteristic time. Figure 7 shows the PDF of $\Delta\tau_1$. The straight lines indicate exponential distributions, and their slopes yield approximately the same characteristic time scale $\tau_m \simeq 400$ s.

The implication of these observations is that the time interval τ_1 assumes a variety of values between 30 s and 400 s, all of which are distributed in a self-similar manner. The two cutoff scales should correspond to specific aspects coming from the physics of the problem that lies outside the hierarchical structure of scales. The meaning of the lower cutoff scale τ_L, already discussed briefly, will be reconsidered in Sec. IV A; an explanation of the upper cutoff τ_M will be given in Sec. IV D.

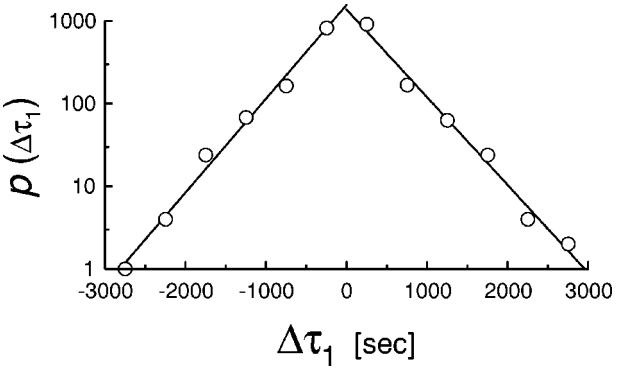

FIG. 7. The PDF of the increments $\Delta\tau_1$ of the interswitch intervals versus $\Delta\tau_1$; Ra$=1.5\times10^{11}$. Straight lines indicate exponential distributions of both positive and negative increments.

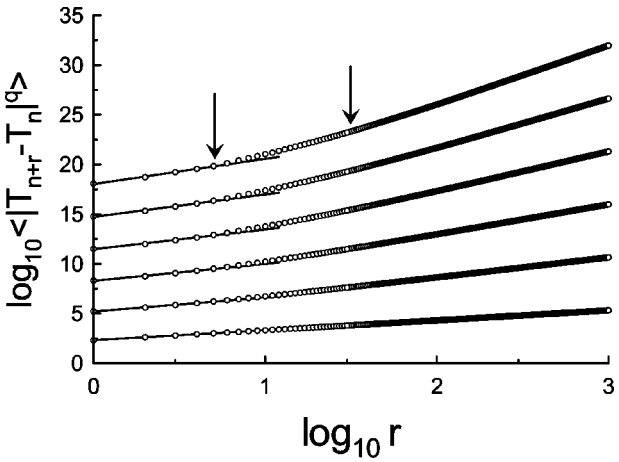

FIG. 8. Moments of the generalized interswitch intervals versus the variable r; Ra$=1.5\times10^{11}$. Upper data sets correspond to increasing order of the moments ($q=1,2,\ldots,6$). The left arrow shows the end of one scaling behavior and the right arrow shows the beginning of another. Straight lines indicate power laws.

B. Finite-size scaling

Because it is difficult to draw definitive conclusions from the analysis of relatively few data points (in spite of the real-time record of 5.5 days), an additional study of the moments of the generalized interswitch intervals (3) proves to be useful. Figure 8 shows the dependence of $\log_{10}\langle\tau_r^q\rangle$ on $\log_{10} r$ for Ra$=1.5\times10^{11}$ for q between 1 and 6 (from bottom to top); here, $\langle\cdot\rangle$ is the running average taken along the sample. One can recognize two scaling regions in this figure, where the scaling dependences

$$\langle\tau_r^q\rangle\sim r^{\zeta_q} \tag{6}$$

are indicated by straight lines. We observe the first scaling region for $r\leqslant5$ and the second scaling for $r>50$. Figure 9 shows the scaling exponents ζ_q for both scaling intervals. The straight lines indicate a linear dependence

$$\zeta_q=\alpha+\beta q. \tag{7}$$

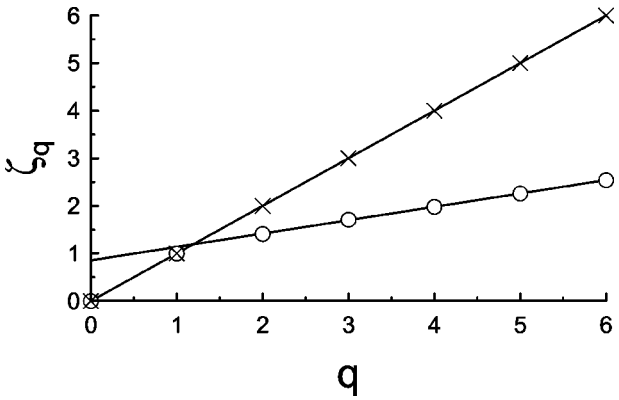

FIG. 9. The scaling exponents ζ_q against the moment order q; Ra$=1.5\times10^{11}$. Crosses correspond to large-scale scaling interval ($r>50$) and circles to small-scale scaling interval ($r<5$). Straight lines mark the linear dependence.

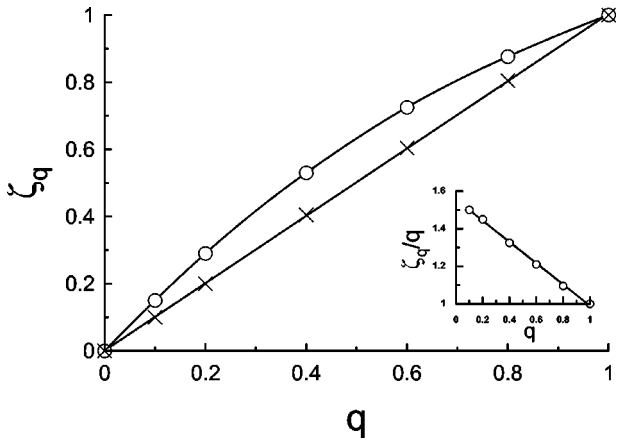

FIG. 10. The scaling exponents ζ_q against order $q \leqslant 1$ (Ra $=1.5\times10^{11}$). Crosses correspond to the large-scale scaling interval ($r>50$), and circles to the small-scale scaling interval ($r<5$). The solid straight lines in the inset represent a lognormal distribution for small values of the generalized interswitch intervals.

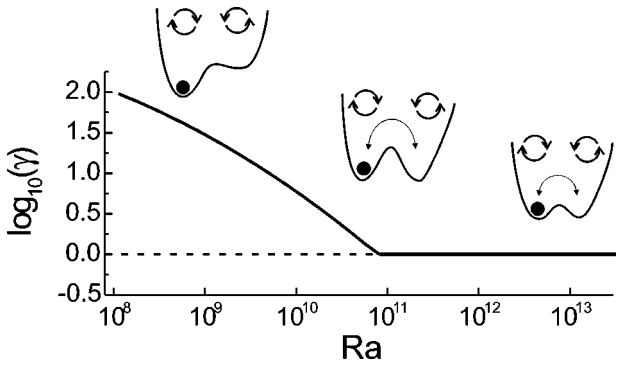

FIG. 11. A schematic of the dynamical model describing the noise-induced switches between the two metastable states of the mean wind, as a function of Ra. For low Ra, the two parts of the potential well are separated by sufficiently strong barriers so there is a preponderance of wind in one direction. At about Ra$=10^{11}$, the two wells become of equal depth. For higher Ra, the barrier height decreases relative to the fluctuation level.

For the scaling in the large-r range, we obtain $\alpha=0$ and $\beta=1$. This property is related to the complete decorrelation of the events for sufficiently large r in Eq. (3). On the other hand, for the range of smaller r, the linear dependence begins for $q=2$, and we have $\alpha\simeq0.85$ and $\beta\simeq0.28$. A standard interpretation of such scaling (with the PDF showing a -1 region) is the so-called finite-size scaling [20]. To describe finite-size scaling one can use the ansatz

$$p(\tau_1)=\frac{r^{\alpha}}{\tau_1}f\left(\frac{r^{\beta}}{\tau_1}\right), \tag{8}$$

where the cutoff function $f(x)$ should describe the behavior of the PDF for small x (i.e., for large τ_1).

The moments for intermediate values of r, namely, $5<r<50$, do not apparently exhibit the usual scaling properties (see Fig. 8). However, utilizing the so-called extended self-similarity (ESS) one can study this interval of r scales as well. Because of its specialized nature, we have relegated this part to the Appendix.

C. Small-scale interswitch intervals

The scaling behavior of low-order moments $q<1$ can be used to study the statistical properties of the shortest interswitch intervals. This behavior cannot be easily captured by examining the PDF alone. Figure 10 shows, on an expanded scale, the exponents ζ_q for $q<1$ for both scaling ranges in r. The symbols in this figure are the same as in Fig. 9. One can see that for large r (crosses) we have the same complete decorrelation of the events as shown in Fig. 9. For small r (circles), the dependence ζ_q on q is nonlinear for $q<1$. The inset in Fig. 10 shows the same data as in the main figure but now we plot ζ_q/q on the ordinate. This figure shows that the data for small r and q can be well fitted by a straight line of the form

$$\zeta_q/q=a+bq. \tag{9}$$

It is well known (see, e.g., Monin and Yaglom [21]) that this type of scaling points to a process with an underlying lognormal distribution.

Before proceeding to interpret these results, we should note that similar results have been obtained for other Rayleigh numbers as well. The analysis is not as detailed, primarily because the data records were shorter. In general, the results are qualitatively the same. Some quantitative results are also the same (e.g., the range of scales for which the -1 power law is valid is about the same), but some are different [e.g., the numerical values of α and β in Eq. (7)].

IV. INTERPRETATION OF RESULTS

A. General

The power-law probability density with a slope of -1, with an exponential cutoff function and a finite-size scaling, is a typical indication of the so-called self-organized criticality or SOC (see, e.g., [22–25] and references cited in them). There could be many possible scenarios of SOC in this complex system where numerous plumes and jets are developed as a result of boundary layer instabilities, all of which are embedded in a background of strong turbulent fluctuations prevalent in the core. It was suggested recently for plasma turbulence (see Refs. [26,27]) that instabilities governed by a threshold may lead to self-organized criticality by producing transport events at all scales, called avalanches. These avalanches are due to local accumulation of energy, leading to an increasing gradient. Once the gradient exceeds the threshold, a burst of activity occurs, which expels the accumulated energy. This process can be renewed, much like a domino effect, leading to a large transport event.

Let us, however, abstract all these complex details and consider a simple dynamical picture with two metastable states divided by an energy barrier. One of the metastable states corresponds to one direction of the wind, while the other metastable state corresponds to the opposite direction. Irregular jumps of the system from one metastable state to the other are due to the action of a ''noise.'' The noise can be

associated with turbulent fluctuations, thermal or otherwise, contained in the system. The height of the barrier (''threshold'') can also fluctuate. A possible schematic of this metastable model is shown in Fig. 11 as a function of Ra. As can be concluded from Sec. II B, the two wells are sufficiently disparate in heights at low Rayleigh numbers, so that there is a preponderance of the wind in one direction. At about Ra $=10^{11}$, the wells apparently become of equal depth, and the system is likely to spend its time equally in the two wells (cf. Fig. 2). Further increase in Ra makes it easier for the system to hop from one well to another, either because the threshold needed for the crossover becomes weaker, or because the noise increases in magnitude. Both these features have the same relative effect.

A noise excitation process leading to crossover of a threshold (and, consequently, to jumps from one metastable state to another) can be described by the well-known Arrhenius-Kramers relationship [28] between typical time τ_1 between crossings and height of the energy threshold (''barrier'') E as

$$\tau_1 \simeq \tau_{10} e^{E/D}, \tag{10}$$

where D is the noise strength. (For the particular case of a thermal excitation process, $D=kT$, where T is the temperature and k is the Boltzmann constant.) Relationship (10) can be considered to apply to wider classes of phenomena than SOC.

If the threshold itself fluctuates with a probability density $p_{th}(E)$, one obtains from Eq. (10) that the distribution of τ_1 is

$$p(\tau_1) = p_{th}(E)\frac{dE}{d\tau_1} = D\frac{p_{th}(\ln \tau_1)}{\tau_1}. \tag{11}$$

A remarkable property of this representation is that for sufficiently broad threshold distributions one can approximately replace (in some interval of scales) the $p_{th}(\ln \tau_1)$ by a constant (in comparison to the τ_1^{-1} form). This leads to the power-law dependence $p(\tau) \sim \tau^{-1}$ in this interval of scales.

It is worth noting as an aside that for the Boltzmann distribution of thresholds

$$p_{th}(E) \sim e^{-E/kT}, \tag{12}$$

by substituting Eq. (12) into Eq. (11) and using Eq. (10), we also obtain a power-law distribution of the interswitch intervals

$$p(\tau_1) \sim \tau_1^{\alpha} \tag{13}$$

with

$$\alpha = -\left(1 + \frac{D}{kT}\right). \tag{14}$$

For weak noise, i.e., for $D/kT \ll 1$, we obtain from Eqs. (13) and (14) the -1 distribution with a slight correction (from our estimate for Ra$=1.5\times 10^{11}$, $D<0.1kT$).

It might be argued with justification that turbulent convection at high Rayleigh numbers is a highly nonequilibrium problem while the Kramers approach, embodied by the Boltzmann-type arguments given in Eqs. (10) and (12), is usually thought to be valid only for systems at or near thermal equilibrium. However, it was shown in a recent work [29] using the Swift-Hohenberg model of Rayleigh-Bénard convection [30] that the Kramers approach can be effectively applied to the longest-lived modes of nonequilibrium systems, even at a finite distance from a bifurcation threshold. The main reason for this is that, close to the bifurcation threshold, there is a good scale separation between fast and slow variations of the amplitudes (cf. the Appendix). Far from the bifurcation threshold, the separation between fast and slow scales does not hold in general, although in the case of the wind, its slow dynamics makes such a separation plausible. Even so, it seems better to treat E in Eq. (10) as the pinning energy for the large-scale motion [29] and D as ''turbulent noise.'' It is shown in [29] that the stochastic Swift-Hohenberg model (i.e., the Swift-Hohenberg equation with the addition of noise [31]) is an example in which the pinning potential barrier can be overcome by stochastic noise, and the problem can be reduced to the Kramers approach for the longest-lived modes.

While the threshold distribution (12) is quite plausible, it cannot be used in Eq. (11) as the cutoff function: an ''intrinsic'' cutoff is absent in the processes considered so far, and one can expect that the real cutoff should be related to external effects that are generally Poisson-like. That is, for large enough τ_1, the distribution should decay exponentially and the characteristic Poisson time scale should be generated by a process unrelated to wind dynamics. We have noted that this time scale is of the order of 400 s. An approximate estimate of the magnitude of the ''external'' Poisson time scale τ_M is given by the upper end of the first finite-size scaling in Fig. 8.

Let us finally consider the log-normal distribution of the small values of generalized interswitch intervals mentioned in Sec. III C. One can expect that for such small time intervals the relatively slow fluctuations of the threshold play no role, and we can consider the situation to be close to *bistable* with a stationary threshold. It was shown, for instance, in a recent paper [32] that for the simplest overdamped bistable oscillator

$$\dot{x} = x - x^3 + \eta(t) \tag{15}$$

[where $\eta(t)$ is the white-noise term], the return times exhibit log-normal multifractal properties. The bistable oscillator given by Eq. (15) was previously used by Villermaux to describe the short-term oscillations in turbulent convection. If we now force this oscillator by a weak periodic input signal $f(t)=A\sin(\Omega t+\phi)$ such that

$$\dot{x} = x - x^3 + \eta(t) + f(t), \tag{16}$$

it is conceivable that a stochastic resonance can take place [32]. In our case the wind circulation itself could be consid-

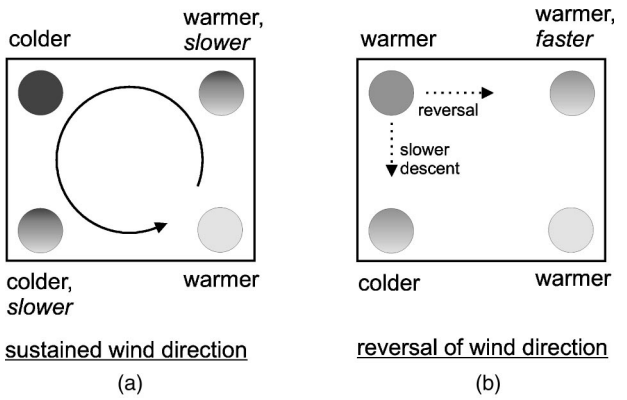

FIG. 12. Schematic of the conditions corresponding to (a) the sustenance of the mean wind, and (b) the reversal of its direction.

ered a periodic input (with the turnover time as a period). This could explain the peak observed in Fig. 5.

B. A physical picture

At present, we do not know enough to provide a definitive account of the wind and its properties. From the analysis of the data discussed so far, we should search for a phenomenon that is self-sustaining but with in-built seeds for reversing itself; the initiation of the reversal, perhaps that of the wind itself, is a ''noise'' effect, interpreted broadly. The interswitch interval is truncated (at about 400 s) by a cutoff process that is yet to be discussed. In addition, we believe that the explanation must be consistent with the mechanism of wind reversals in a closed tube carrying fluid heated from below (Refs. [33–36]). In particular, it should be consistent with the main conclusion of Ref. [33] that the wind reversal is essentially a matter of balance between buoyancy and friction, with inertia playing only a secondary role. We now combine these essential features to paint a rough physical picture, with full awareness that more work is required to sharpen it.

The following discussion is best presented with reference to Fig. 12. Imagine a parcel of fluid, which arrives at the bottom right corner [Fig. 12(a)], and is slightly warmer than the ambient fluid. According to our understanding from the previous section, the reason for this heating is likely to be stochastic in nature. Because the parcel is warmer than its neighbors, it will correspondingly rise with greater speed. One *plausible* result of this faster and upward mobility is that the increased friction on the fluid parcel slows it down by the time it arrives at the top right corner, still warmer than its new surroundings. If so, this fluid parcel, being warmer and slower than its neighboring fluid elements, as it moves horizontally to the left, has a better chance of losing its thermal energy to the top plate, which is maintained cold. The result is that by the time it arrives at the top left corner, the fluid parcel will be colder than its neighboring fluid elements. If so, it will sink more easily downward to bottom left, and a sustained wind becomes possible.

The key to this scenario is that the fluid parcel should arrive at top right from bottom right in a state that is both warmer and slower than its surroundings. This is possible if the retardation due to friction more than balances the enhanced buoyancy of the fluid parcel at bottom right. If on the other hand, as might happen at higher Rayleigh numbers [see Fig. 12(b)], the enhanced buoyancy is large enough that the decelerating effect of the friction is unable to slow down the fluid parcel, it arrives at the top right corner in a state that is both warmer and faster than its neighboring fluid elements. If so, it is conceivable that the heat transfer between the fluid parcel in question and the top wall is not as efficient, during the horizontal motion, as in the previous case. The fluid parcel may arrive at top left in a warmer state than its neighbors. This will make the fluid parcel susceptible to traversing down the sidewall with a slower speed, or, in the extreme case, reverse its direction.

We shall now consider the cutoff time scale of about 400 s, and argue that it is related in a subtle manner to sidewall effects. In principle, this will complete the picture.

C. Sidewall effects and the upper cutoff scale

In the present apparatus, the sidewall can be regarded as an excellent insulator not only because the stainless steel is a poor conductor at low temperature, but also because the convection chamber is housed in three other vacuum shields, each of which has been evacuated to diminishingly low pressures. The conduction of heat across the sidewalls is therefore negligible. On the other hand, this does not preclude a small fraction of heat from being conducted along the sidewall from the bottom to the top plate. This fraction is proportional to the ratio of the conductivity of the sidewall to the effective conductivity of the gas in the convection chamber. Typically, experimentalists account for this fact by subtracting from the measured heat transport a fraction of heat that is estimated to be transported along the container sidewalls. This estimate is made from measurements in the empty cell. As pointed out by Ahlers [37] and Roche *et al.* [38], this procedure is not likely to be correct in detail because the nature of heat transfer along the sidewall depends on the state of the boundary layers, which itself changes with Ra.

For high Ra, the sidewall effect just described is likely to be small because the effective conductivity of the fluid is enhanced by the factor of the Nusselt number. At low Rayleigh numbers, however, the effect may not be negligible. Plausible but rough estimates suggest that the fraction of heat conducted along the sidewalls lies somewhere between 2% and 7% for the present conditions [37–39]. Even this modest effect could have a large influence on wind reversals. We infer that this might be so from the following test.

We added an insulating layer of polyethylene terephthalate (Mylar) to the entire inner surface of the stainless steel sidewall. The Mylar strip was 0.127 mm thick. The flange region of the joints just above the lower plate and below the upper plate was covered with an additional 2.5 cm wide strip of Mylar of the same thickness. This extra insulating layer completely covered the vertical extent of the stainless steel flanges. The Mylar sheet was bonded to the sidewall by a thin layer of low-viscosity Stycast 1266 epoxy. A small fraction of the inner surface at the weld joint was not covered by

Mylar but that too was coated with insulating epoxy. From Ref. [40], we estimate the conductivity of polyethylene terephthalate to be $k=0.02\pm0.005$ W/m K at a temperature of 5 K (using a linear extrapolation from 28 K in $\log k$–$\log T$). The conductivity of the type 304 stainless steel at the same temperature (see Ref. [19]) is approximately 0.25 W/m K. The sidewall resistance is thus believed to have increased by an order of magnitude with respect to lateral conduction between the fluid and the sidewall, and by a factor of about 2 with respect to conduction along its height between the bottom and top plates. The latter is the more relevant factor here.

By making this modest change, we found that the wind reversal had been changed as follows: the onset of reversals was postponed to a higher Rayleigh number, and, at the Rayleigh number of 1.5×10^{11}, although reversals still occurred, the mean wind tended to show a preference for one direction over the other. The phenomenon appears to be the same as before, but shifted to higher Rayleigh numbers. This shows that the sidewall has some bearing on the wind reversals.

If we include this qualitative fact in the discussion of Sec. IV B, the following picture seems to emerge. The sidewall temperature at the bottom of the container can be expected to vary from the bottom to the midplane in an exponential manner. This has a certain characteristic thickness—corresponding, for example, to the $1/e$ factor of the total temperature difference. Denote this thickness by λ. This thickness can be estimated (e.g., Ref. [38]) as $(k_w t d/k_f)^{1/2}$, where k_w and k_f are the thermal conductivities of the wall and the fluid, t is the sidewall thickness, and d is the boundary layer thickness on the sidewall. For the present conditions, $\lambda=1.2$ cm. This length scale may define the size of the ''corner eddies'' of the cell presented to the wind. The characteristic diffusion time associated with this corner region of the fluid is approximately 300 s, of the same order as 400 s mentioned earlier for τ_M.

Assuming that this correspondence is not a coincidence, we can interpret it in the following manner. A wind reversal requires a ''kick'' to cross the barrier in the double-well potential of Fig. 11. In general, the fluid parcels are not in equilibrium with the sidewall, and so the magnitude of the perturbation required will be finite. If, however, the wind has been established in one direction for a long time so it equilibrates with the wall, the perturbation required will be infinitesimally small, and so almost any disturbance will make the fluid parcel change its direction (Poisson-like conditions). Thus, the longest time scale involved in the wind's sustenance in one direction is the time required for sidewall equilibration to occur. This seems to be of the order of the time taken for the sidewall temperature distribution to be stabilized.

V. CONCLUDING REMARKS

Among the myriad details of thermal convection at high Rayleigh numbers [7], an aspect that invites attention is the mean wind and its propensity to reverse its direction apparently irregularly. In spite of the extraordinary complexity of the processes involved, and in spite of the paucity of detailed measurements, it is possible to deduce some basic features of the wind and its reversal. The basic physics appears to be an imbalance between buoyancy and friction, with inertia playing a secondary role. (Free-fall conditions do not prevail in the regions close to the walls.) In this apparently bistable system, the ''noise'' needed for overcoming the barrier can be naturally associated with the background thermal turbulence. Using this simple model one can explain the main features of wind reversal. In broad terms, the existence of the -1 power-law probability distribution of the interswitch time intervals, finite-size scaling, and exponential cutoff of the PDFs can be regarded as the signatures of self-organized criticality. If this scenario is valid, we may consider the ''avalanche'' mechanism to be provided by various boundary layer instabilities, jets, and plumes, none of whose dynamics we understand fully.

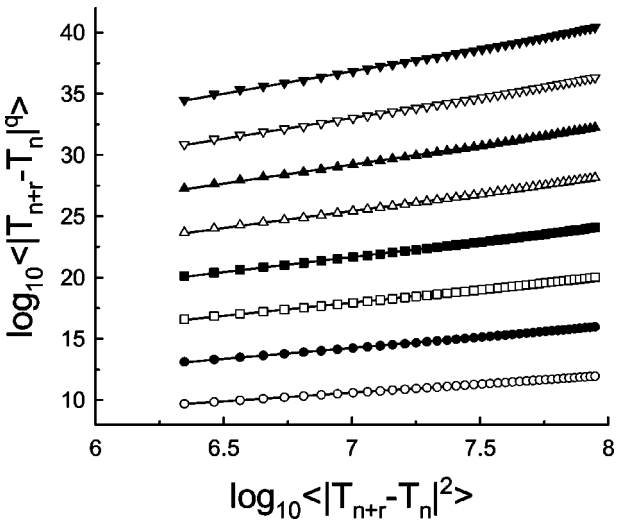

FIG. 13. Moments of the generalized interswitch intervals versus r ($\mathrm{Ra}=1.5\times10^{11}$), plotted against the second order moment. Upper data sets correspond to the increasing order of the moments ($q=3,4,\ldots,10$). The straight lines indicate the scaling behavior.

ACKNOWLEDGMENTS

The authors are grateful to R. J. Donnelly and L. Skrbek for their role in the experiment, to D. Fukayama for help in calculations, and to J. Schumacher for useful discussions. The work was supported by the NSF through Grant No. DMR-95-29609.

APPENDIX

The moments of the generalized interswitch interval (3) do not exhibit scaling in the interval $5<r<50$ (Fig. 8). However, one can observe the extended self-similarity in this interval of scales, as shown in Fig. 13. Straight lines drawn in the figure indicate the generalized scaling

$$\langle \Delta T_r^q \rangle \sim \langle \Delta T_r^2 \rangle^{\mu_q}. \tag{A1}$$

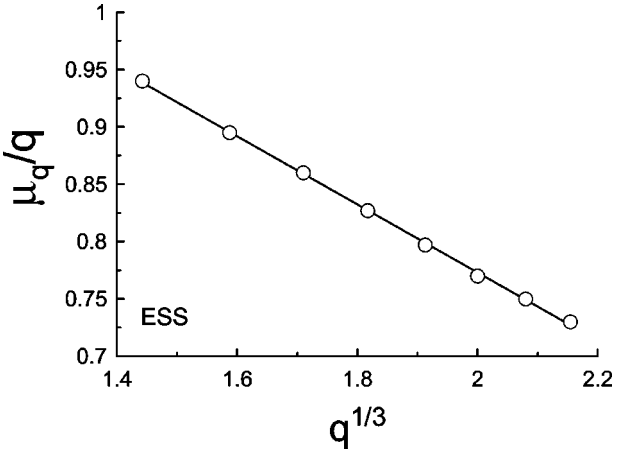

FIG. 14. The ESS exponents μ_q/q against $q^{1/3}$. The solid straight line (the best fit) is drawn to indicate the behavior (A3) characteristic of bilognormal distributions.

This is the extended self-similarity (see Ref. [41]); if ordinary self-similarity, which subsumes ESS, holds, one would have

$$\mu_q = \frac{\zeta_q}{\zeta_2}. \tag{A2}$$

Figure 14 shows μ_q/q extracted from Fig. 13 against $q^{1/3}$. The straight line is drawn in this figure to indicate the dependence

$$\mu_q/q = \alpha + \beta q^{1/3}. \tag{A3}$$

Using the saddle-point approximation (see, for instance, Refs. [42–44]) one can show that just this dependence of μ_q on q (for large enough q) corresponds to a bilognormal distribution of the generalized interswitch intervals,

$$p([\ln \tau]^2) \sim \exp - \left[\frac{([\ln \tau]^2 - m)^2}{\sigma^2} \right], \tag{A4}$$

where m and σ are some constants. To check this result, we calculated directly the PDFs of $[\ln \tau]^2$ for $r = 6, 8, 10$, and 20. The results are shown in Fig. 15. The axes in this figure are semilogarithmic, so that the parabolas drawn as best fits to the data indicate the bilognormal distribution (A4). It should be noted that the bistable systems with fixed threshold under noise action exhibit lognormal behavior for their return time sequences (see the end of Sec. IV A). For large

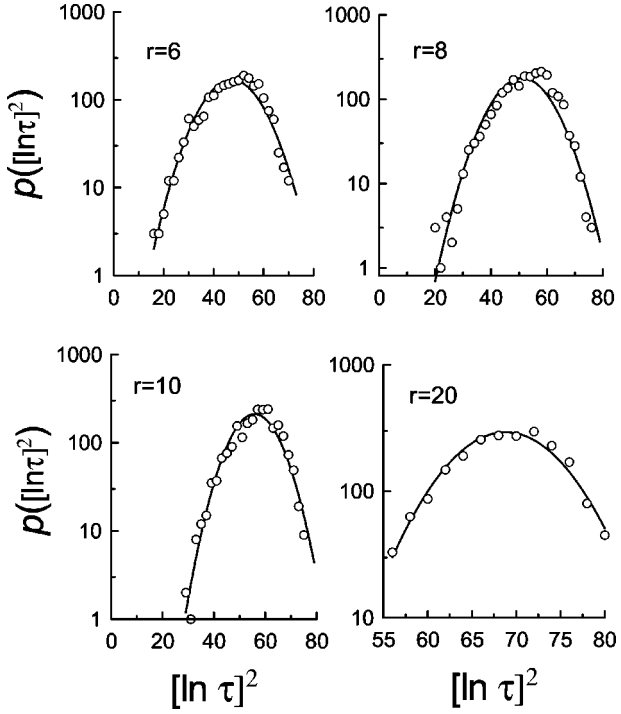

FIG. 15. The PDF of $[\ln \tau_r]^2$ (where $\tau_r = T_{n+r} - T_n$) versus $[\ln \tau_r]^2$ for different values of r; $\mathrm{Ra} = 1.5 \times 10^{11}$. The solid parabolas (the best fit) indicate the bilognormal distribution (A4).

interswitch intervals the threshold fluctuations should play a significant role, and one should seek another explanation for Eq. (A4).

If, for some reason, the fluctuating thresholds are statistically *increasing* with time, then the sequence of the $r-1$ interswitch intervals, $\tau_1, \tau_2, \ldots, \tau_{r-1}$, composing the generalized interswitch interval $\Delta T_r = T_{n+r} - T_n$, although statistically independent, form a cluster (climbing on the staircase of increasing barriers). Equation (10) in this case gives us the relationship

$$\Delta T_r = \tau_1 \cdot \tau_2 \cdots \tau_{r-1}. \tag{A5}$$

Taking the logarithm of both sides of this equation we obtain

$$\ln \Delta T_r = \ln \tau_1 + \ln \tau_2 + \cdots + \ln \tau_{r-1}. \tag{A6}$$

If the central limit theorem can be applied to this sequence we obtain a lognormal distribution of the generalized interswitch intervals for sufficiently large r. The bilognormal distribution then appears as a result of self-averaging over subclusters.

[1] R. Krishnamurti and L.N. Howard, Proc. Natl. Acad. Sci. U.S.A. **78**, 1981 (1981).
[2] M. Sano, X.-Z. Wu, and A. Libchaber, Phys. Rev. A **40**, 6421 (1989).
[3] B. Castaing, G. Gunaratne, F. Heslot, L. Kadanoff, A. Libchaber, S. Thomae, X.-Z. Wu, S. Zaleski, and G. Zanetti, J. Fluid Mech. **204**, 1 (1989).
[4] S. Ciliberto, S. Cioni, and C. Laroche, Phys. Rev. E **54**, R5901 (1996).
[5] S. Grossmann and D. Lohse, J. Fluid Mech. **407**, 27 (2000).
[6] X.-L. Qiu, S.-H. Yao, and P. Tong, Phys. Rev. E **61**, R6075 (2000).
[7] L. Kadanoff, Phys. Today **54**(8), 34 (2001).
[8] J.J. Niemela, L. Skrbek, K.R. Sreenivasan, and R.J. Donnelly,

J. Fluid Mech. **449**, 169 (2001).
[9] S. Grossmann (private communication).
[10] G.A. Glatzmeier, R.C. Coe, L. Hongre, and P.H. Roberts, Nature (London) **401**, 885 (1999).
[11] E. van Doorn, B. Dhruva, K.R. Sreenivasan, and V. Cassella, Phys. Fluids **12**, 1529 (2000).
[12] X.-L. Qiu and P. Tong, Phys. Rev. E **64**, 036304 (2001).
[13] J.J. Niemela, and K.R. Sreenivasan (unpublished).
[14] A. Belmonte, A. Tilgner, and A. Libchaber, Phys. Rev. Lett. **70**, 4067 (1993).
[15] X. Chavanne, F. Chilla, B. Chabaud, B. Castaing, and B. Hebral, Phys. Fluids **13**, 1300 (2001).
[16] S. Cioni, S. Ciliberto, and J. Sommeria, Dyn. Atmos. Oceans **24**, 117 (1996).
[17] E. Villermaux, Phys. Rev. Lett. **75**, 4618 (1995).
[18] J.J. Niemela, L. Skrbek, K.R. Sreenivasan, and R.J. Donnelly, Nature (London) **404**, 837 (2000).
[19] Brookhaven National Laboratory Report, BNL 10200-R, Vol. 1 (Associated Universities, Inc., Brookhaven, NY).
[20] C. Tebaldi, M. De Menech, and A.L. Stella, Phys. Rev. Lett. **83**, 3952 (1999).
[21] A.S. Monin and A.M. Yaglom, *Statistical Fluid Mechanics: Mechanics of Turbulence* (MIT Press, Cambridge, MA, 1975), Vol. 2.
[22] P. Bak, *How Nature Works* (Copernicus, New York, 1996).
[23] H.J. Jensen, *Self-organized Criticality* (Cambridge University Press, Cambridge, England, 1998).
[24] R. Pastor-Satorras and A. Vespignani, Phys. Rev. E **61**, 4854 (2000).
[25] M. De Menech and A.L. Stella, Phys. Rev. E **62**, R4528 (2000).
[26] P.H. Diamond and T.S. Hahm, Phys. Plasmas **2**, 3640 (1995).
[27] B.A. Carreras, D. Newman, V.E. Lynch, and P.H. Diamond, Phys. Plasmas **3**, 2903 (1996).
[28] H.A. Kramers, Physica (Amsterdam) **7**, 284 (1940).
[29] D. Boyer and J. Vinals, e-print cond-mat/0110254.
[30] J. Swift and P.C. Hohenberg, Phys. Rev. A **15**, 319 (1977).
[31] G. Ahlers, M. Gross, P.C. Hohenberg, and S. Safran, J. Fluid Mech. **110**, 297 (1981).
[32] A. Silchenko and C-K. Hu, Phys. Rev. E **63**, 041105 (2001).
[33] J.B. Keller, J. Fluid Mech. **26**, 599 (1966).
[34] P. Welander, J. Fluid Mech. **29**, 17 (1967).
[35] M. Gorman, P.J. Widmann, and K.A. Robbins, Phys. Rev. Lett. **52**, 2241 (1984).
[36] A.G. Tomboulides and V. Yakhot, Phys. Rev. E **63**, 035304 (2001).
[37] G. Ahlers, Phys. Rev. E **63**, 015303 (2001).
[38] P.-E. Roche, B. Castaing, B. Chabaud, B. Hebral, and J. Sommeria, Eur. Phys. J. B **24**, 405 (2001).
[39] K.R. Sreenivasan and J.J. Niemela (unpublished).
[40] G.E. Childs, L.J. Ericks, and R.L. Powell, *Thermal Conductivity of Solids at Room Temperature and Below: A Review and Compilation of the Literature*, Natl. Bur. Stand. Monograph No. 131 (U.S. GPO, Washington, DC, 1973), p. 533.
[41] R. Benzi, L. Biferale, S. Ciliberto, M.V. Struglia, and R. Tripiccione, Physica D **96**, 162 (1996).
[42] A. Bershadskii, Europhys. Lett. **53**, 716 (2001).
[43] M.K. Georgoulis and L. Vlahos, Astron. Astrophys. **336**, 721 (1998).
[44] A.L. MacKinnon and K.P. Macpherson, Astron. Astrophys. **326**, 1228 (1997).